

# Finite Element Analysis of Three-Dimensional Superelastic Behaviors of Shape Memory Alloy Devices

Daegon CHOI and Yutaka TOI

**Abstract**—The three-dimensional incremental finite element formulation previously developed for the multiaxial behaviors of shape memory alloy devices by authors is extended to the geometrically nonlinear analysis and applied to the analyses on the superelastic behaviors of SMA devices. The calculated results are compared with the experimental results in the literature to illustrate the validity of the proposed computational modeling. It is expected that the present three-dimensional finite element tool will be useful to predict the superelastic behaviors of various shape memory alloy devices.

**Index Terms**—Shape Memory Alloys, Finite Element Method, Structure Analysis, Superelasticity, Computational Mechanics.

## I. INTRODUCTION

The shape memory alloys (abbreviated as SMAs) have been extensively studied as functional materials for a variety of applications, including medical, structural, and other advanced devices. The SMAs have the superelasticity (shape recovery by the unloading) as well as the shape memory effect (shape recovery by the heating). Elements which are formed out of these materials are typically subjected to multiaxial stress-states during their operation. The development of a computational tool to support the design process is necessary for the efficient development of the SMA devices with a complicated shape and mechanical characteristics.

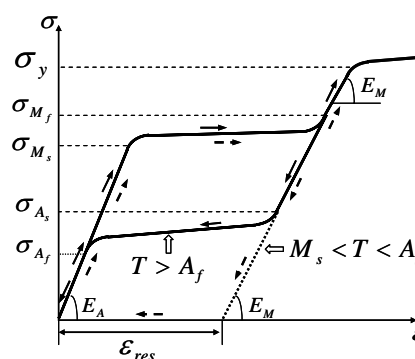
Since the discovery of the shape memory alloys in the 1960s, researchers have been investigating both experimental aspects of their behaviors as well as their constitutive modeling. Auricchio [1], Lim and McDowell [2], Dettmer and Reese [3], Auricchio and Petrini [4], Pan, Thamburaja, and Chau [5], Reese and Christ [6] formulated the constitutive equations of the SMAs, some of which have been applied to the finite element analysis. However, the standard computational procedure has not yet been established.

The authors proposed a method of finite element analysis for the multiaxial behaviors of SMA devices of three-

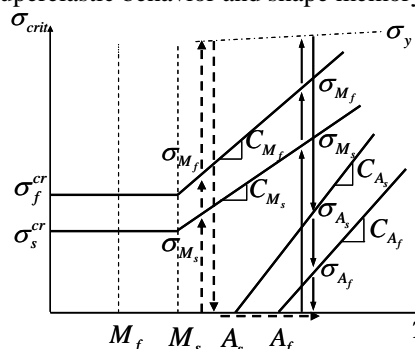
dimensional shape and experimentally verified the validity of the proposed method [7]. In the present study, the proposed method is extended to the geometrically nonlinear analysis and applied to the analyses on the superelastic behaviors of a SMA microtube, a SMA column, and a SMA stent. The calculated results are compared with the experimental results to show the validity of the proposed constitutive modeling.

## II. CONSTITUTIVE EQUATION OF THE SMAS

The mechanical properties of the SMAs discussed in the present study are schematically shown in Fig. 1. Fig. 1(a) shows the superelastic behavior (bold line arrow) and the shape memory effect (dotted line arrow), while Fig. 1(b) is the relation between the critical transformation stresses and the temperature. The following notations are used in Fig. 1:  $\sigma$ ; the stress,  $\varepsilon$ ; the strain,  $T$ ; the temperature,  $\sigma_f^{cr}$  and  $\sigma_s^{cr}$ ; the critical stresses for finishing and starting martensite transformation,  $M_f$  and  $M_s$ ; the temperatures for finishing and starting martensite transformation,  $A_s$  and  $A_f$ ; the temperatures for starting and finishing austenite transformation.



(a) Superelastic behavior and shape memory effect



(b) Critical stresses for transformation vs. temperature  
 Fig. 1 Mechanical properties of shape memory alloys

Manuscript received December 8, 2008.

D. Choi is with Institute of Industrial Science, the University of Tokyo 4-6-1 Komaba, Meguro-ku, Tokyo, 153-8505 JAPAN (e-mail: dgonchoi@iis.u-tokyo.ac.jp).

Y. Toi is with Institute of Industrial Science, the University of Tokyo 4-6-1 Komaba, Meguro-ku, Tokyo, 153-8505 JAPAN (corresponding author to provide phone: 81-3-5452- 6178; fax: 81-3-5452-6180; e-mail: toi@iis.u-tokyo.ac.jp).

The superelastic behavior as shown in Fig. 1(a) occurs, when the stress loading and unloading take place at the constant temperature higher than  $A_f$  in Fig. 1(b).  $C_{M_s}$  and  $C_{M_f}$  are the gradients of the critical stresses for starting and finishing martensite transformation with respect to the temperature, while  $C_{A_s}$  and  $C_{A_f}$  are the gradients of the critical stresses for starting and finishing austenite transformation with respect to the temperature.

The formal extension of the one-dimensional stress-strain relation for the SMAs leads to the three-dimensional modeling as given by the following equations:

$$\{\sigma\} = [D]\{\varepsilon\} + \xi_s \{\Omega\} + T\{\theta\} \quad (1)$$

$$\{\sigma\}^T = [\sigma_x \quad \sigma_y \quad \sigma_z \quad \tau_{xy} \quad \tau_{yz} \quad \tau_{zx}] \quad (2)$$

$$\{\varepsilon\}^T = [\varepsilon_x \quad \varepsilon_y \quad \varepsilon_z \quad \gamma_{xy} \quad \gamma_{yz} \quad \gamma_{zx}] \quad (3)$$

where the following notations are used:  $\{\sigma\}$ ; the stress vector,  $\{\varepsilon\}$ ; the strain vector,  $[D]$ ; the stress-strain matrix,  $\{\Omega\}$ ; the transformation vector,  $\xi_s$ ; the stress-induced martensite volume fraction,  $\{\theta\}$ ; the thermal elastic coefficient and  $T$ ; the temperature.

The stress-strain matrix  $[D]$  is given by the following equation:

$$[D] = \frac{E}{(1+\nu)(1-2\nu)} \times \begin{bmatrix} 1-\nu & \nu & \nu & 0 & 0 & 0 \\ \nu & 1-\nu & \nu & 0 & 0 & 0 \\ \nu & \nu & 1-\nu & 0 & 0 & 0 \\ 0 & 0 & 0 & \frac{1-2\nu}{2} & 0 & 0 \\ 0 & 0 & 0 & 0 & \frac{1-2\nu}{2} & 0 \\ 0 & 0 & 0 & 0 & 0 & \frac{1-2\nu}{2} \end{bmatrix} \quad (4)$$

where  $E$  and  $\nu$  are Young's modulus and Poisson's ratio, respectively. Young's modulus  $E$  is expressed by the following equation as a function of the total martensite volume fraction  $\xi$ :

$$E = E_a + \xi(E_m - E_a) \quad (5)$$

where  $E_m$  and  $E_a$  are Young's modulus of the martensite phase and the austenite phase, respectively.

The total martensite volume fraction  $\xi$  is expressed as follows:

$$\xi = \xi_s + \xi_T \quad (6)$$

where  $\xi_T$  is the temperature-induced martensite (twinned martensite) volume fraction.  $\xi$ ,  $\xi_s$ , and  $\xi_T$  are all functions of the temperature and the stresses.

The transformation vector  $\{\Omega\}$  is expressed as follows, using the maximum residual strain vector  $\{\varepsilon_L\}$  and the residual strain direction matrix  $[R_s]$ :

$$\{\Omega\} = -[D][R_s]\{\varepsilon_L\} \quad (7)$$

The maximum residual strain vector  $\{\varepsilon_L\}$  is expressed as follows:

$$\{\varepsilon_L\}^T = [\varepsilon_L \quad \varepsilon_L \quad \varepsilon_L \quad \gamma_L \quad \gamma_L \quad \gamma_L] \quad (8)$$

where  $\varepsilon_L$  and  $\gamma_L$  are the maximum residual normal strain and the maximum residual shear strain, respectively.

The residual strain direction matrix  $[R_s]$  is given by the following equation expressed in terms of the stress components:

$$[R_s] = \begin{bmatrix} \frac{\partial \sigma_{eq}}{\partial \sigma_x} & 0 & 0 & 0 & 0 & 0 \\ 0 & \frac{\partial \sigma_{eq}}{\partial \sigma_y} & 0 & 0 & 0 & 0 \\ 0 & 0 & \frac{\partial \sigma_{eq}}{\partial \sigma_z} & 0 & 0 & 0 \\ 0 & 0 & 0 & \frac{\partial \sigma_{eq}}{\partial \tau_{xy}} & 0 & 0 \\ 0 & 0 & 0 & 0 & \frac{\partial \sigma_{eq}}{\partial \tau_{yz}} & 0 \\ 0 & 0 & 0 & 0 & 0 & \frac{\partial \sigma_{eq}}{\partial \tau_{zx}} \end{bmatrix} \quad (9)$$

where  $\sigma_{eq}$  is von Mises equivalent stress.

The thermo-elastic coefficient vector  $\{\theta\}$  is expressed as follows:

$$\{\theta\} = -[D]\{\alpha\} \quad (10)$$

where the thermal expansion coefficient vector  $\{\alpha\}$  is given as follows:

$$\{\alpha\}^T = [\alpha \quad \alpha \quad \alpha \quad 0 \quad 0 \quad 0] \quad (11)$$

Drucker-Prager equivalent stress is used instead of von Mises equivalent stress in the evolution equation for  $\xi$ ,  $\xi_s$ , and  $\xi_T$  in order to consider the asymmetric tensile and compressive behaviors.

Details of the evolution equation for the martensite transformation process and the inverse austenite transformation process are given by Toi and Choi [7].

### III. FINITE ELEMENT FORMULATIONS

The stress-strain relation (1) is rewritten to the following incremental form of equation to formulate the incremental finite element procedure by the tangential stiffness method:

$$\{\Delta\sigma\} = [D]\{\Delta\varepsilon\} + [\Delta D]\{\varepsilon\} + \Delta\xi_s \{\Omega\} + \xi_s \{\Delta\Omega\} + \Delta T\{\theta\} + T\{\Delta\theta\}$$

$$\begin{aligned}
 &= [D]\{\Delta\varepsilon\} + \Delta\xi[AD_1]\{\varepsilon\} - \Delta\xi_s[D][R_s]\{\varepsilon_L\} \\
 &\quad - \xi_s\Delta\xi[AD_1][R_s]\{\varepsilon_L\} - \xi_s[D][\Delta R_s]\{\varepsilon_L\} \\
 &\quad - \Delta T[D]\{\alpha\} - T\Delta\xi[AD_1]\{\alpha\}
 \end{aligned} \tag{12}$$

where

$$[\Delta D] = \Delta\xi[AD_1] \tag{13}$$

$$[\Delta R_s]\{\varepsilon_L\} = [\Delta R_s\varepsilon_L]\{\Delta\sigma\} \tag{14}$$

Using  $\Delta\sigma^{DP}$ ,  $\Delta\xi$ , and  $\Delta\xi_s$  are expressed as follows:

$$\Delta\xi = A_1[\sigma^{DP}]\{\Delta\sigma\} + A_2\Delta T \tag{15}$$

$$\Delta\xi_s = B_1[\sigma^{DP}]\{\Delta\sigma\} + B_2\Delta T \tag{16}$$

Substituting (15) and (16) into (12), the incremental stress-strain relation is expressed by the following equation:

$$\begin{aligned}
 \{\Delta\sigma\} &= [X]^{-1}[D]\{\Delta\varepsilon\} + [X]^{-1}[Y]\Delta T \\
 &= [D_T]\{\Delta\varepsilon\} + [\Theta_T]\Delta T
 \end{aligned} \tag{17}$$

where  $[X]$  and  $[Y]$  are defined by the following equations:

$$\begin{aligned}
 [X] &= [I] - (A_1[AD_1]\{\varepsilon\}[\sigma^{DP}] - B_1[D][R_s]\{\varepsilon_L\}[\sigma^{DP}] \\
 &\quad - A_1\xi_s[AD_1][R_s]\{\varepsilon_L\}[\sigma^{DP}] - A_1T[AD_1]\{\alpha\}[\sigma^{DP}] \\
 &\quad - \xi_s[D][\Delta R_s\varepsilon_L])
 \end{aligned} \tag{18}$$

$$\begin{aligned}
 [Y] &= A_2[AD_1]\{\varepsilon\} - B_2[D][R_s]\{\varepsilon_L\} - [D]\{\alpha\} \\
 &\quad - A_2\xi_s[AD_1][R_s]\{\varepsilon_L\} - A_2T[AD_1]
 \end{aligned} \tag{19}$$

Details of the finite element formulation described above are given by Toi and Choi [7].

The incremental relation between Green's strains and nodal displacements is written in a matrix form as follows:

$$\{\Delta\varepsilon\} = [\bar{B}]\{\Delta u\} = ([B_0] + [B_L])\{\Delta u\} \tag{20}$$

where the following notations are used:  $[\bar{B}]$ ; the strain-nodal displacement matrix,  $[B_0]$ ; the strain-nodal displacement matrix without the initial displacement,  $[B_L]$ ; the strain-nodal displacement matrix containing the initial displacement,  $\{\Delta u\}$ ; the nodal displacement increment vector.

The following element stiffness equation in an incremental form is obtained by the finite element formulation based on the total Lagrangian approach using the incremental constitutive equation (17).

$$\begin{aligned}
 ([K_0] + [K_T] + [K_G])\{\Delta u\} &= \{\Delta f\} + \{f_R\} \\
 &\quad - \int_V [\bar{B}]^T [\Theta_T]\Delta T dV
 \end{aligned} \tag{21}$$

where

$$[K_0] = \int_V [B_0]^T [D_T][B_0] dV \tag{22}$$

$$\begin{aligned}
 [K_L] &= \int_V ([B_0]^T [D_T][B_L] + [B_L]^T [D_T][B_0] \\
 &\quad + [B_L]^T [D_T][B_L]) dV
 \end{aligned} \tag{23}$$

$$[K_G] = \int_V [G]^T [S][G] dV \tag{24}$$

The following symbols are used:  $[K_0]$ ; the incremental stiffness matrix,  $[K_L]$ ; the initial displacement matrix,  $[K_G]$ ; the initial stress matrix,  $\{\Delta f\}$ ; the external force increment vector,  $\{f_R\}$ ; the unbalanced force vector,  $[D_T]$ ; the superelastic stress-strain matrix,  $[G]$ ; the gradient matrix,  $[S]$ ; the initial stress matrix, and  $V$ ; the element volume. The three-dimensional, eight node isoparametric element is used in the analysis.

#### IV. RESULTS OF FINITE ELEMENT ANALYSIS

##### A. Multiaxial behavior of the SMA microtube

In the present subsection, the calculated results for the SMA microtube (56.0Ni-44.0Ti (at. %)) under an axial force and torsion are compared with the experimental results given by Sun and Li [8].

The material constants used in the analysis are shown in Table 1. The elastic constants of the austenite phase and the temperatures for the phase transformation in Table 1 are from the literature [8], while the other material constants have been determined so as to fit the constitutive equation proposed in the section II with the experimental results [8]. The temperature in the analysis is 23°C which is higher than the temperature for finishing austenite transformation ( $A_f$ ).

Fig. 2(a) shows the dimensions and the boundary conditions of the SMA bar for the uniaxial tensile analysis.

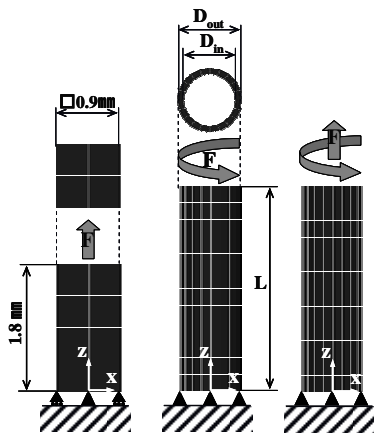
Table 1 Material constants of the SMA microtube (56.0Ni-44.0Ti (at. %)) (\*: Reference [8])

|                             |                       |         |
|-----------------------------|-----------------------|---------|
| Moduli                      | $E_a$ (MPa)           | 30000 * |
|                             | $E_m$ (MPa)           | 20000   |
|                             | $C_{M_s}$ (MPa / °C)  | 5.7     |
|                             | $C_{M_f}$ (MPa / °C)  | 5.7     |
|                             | $C_{A_s}$ (MPa / °C)  | 8.5     |
|                             | $C_{A_f}$ (MPa / °C)  | 36.0    |
|                             | $\nu$                 | 0.3     |
|                             | $\beta$               | 0.15    |
| Transformation Temperatures | $M_f$ (°C)            | -67.6 * |
|                             | $M_s$ (°C)            | -54.2 * |
|                             | $A_s$ (°C)            | -3.26 * |
|                             | $A_f$ (°C)            | 17.4 *  |
| Critical stresses           | $\sigma_s^{cr}$ (MPa) | 0.0     |
|                             | $\sigma_f^{cr}$ (MPa) | 20.0    |
| Maximum residual strains    | $\varepsilon_L$       | 0.044   |
|                             | $\gamma_L$            | 0.044   |

The numbers of elements and nodes are 16 and 45, respectively. The calculated and experimental stress-strain curves are shown in Fig. 3.

Fig. 2(b) shows dimensions ( $L = 5.0\text{mm}$ ,  $D_{out} = 1.5\text{mm}$ ,  $D_{in} = 1.2\text{mm}$ ) and the boundary conditions of the SMA microtube for the torsional deformation analysis. The numbers of elements and nodes are 240 and 520, respectively. The calculated and experimental stress-strain curves are shown in Fig. 4. The perfect superelastic behavior is observed as in the uniaxial tensile analysis as the temperature is  $23^\circ\text{C}$  which is higher than  $A_f$ . The agreement between the calculation and the experiment is not so good as in the uniaxial tensile analysis. In the torsional analysis, the shear modulus  $G$  for the austenite phase is assumed to be 18GPa referring to Sun and Li [8], which does not correspond to the isotropic relation of the material ( $G = E / 2(1 + \nu)$ ). This is probably due to the effect of the anisotropy at the crystal scale as the specimen is very small.

The boundary conditions for the tensile-torsional analysis are shown in Fig. 2(c). Fig. 5 shows the interaction curves of the critical stresses for martensite transformation given by the experiment of Sun and Li [8] and the model proposed in the present study. For comparison, von Mises equivalent stress curve is also shown with a bold line. Although the experimental results are only for the tensile side, it is observed that agreement between the model and the experiment is good when the normal stress is dominant. When the shear stress is dominant, there is about 30% difference at the maximum. This difference is probably due to the effect of anisotropy in small specimens [7].



(a) Uniaxial (b) Torsional (c) Multiaxial

Fig. 2 Finite element models and boundary conditions

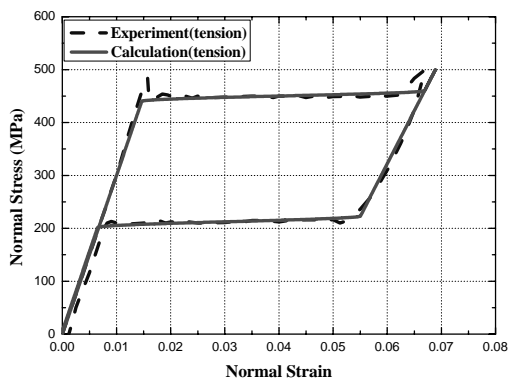


Fig. 3 Normal stress-normal strain curves of SMA bar under uniaxial tension

### B. Buckling behavior of the SMA column

The buckling analysis of the SMA column (40.8Ni-49.3Ti-9.9Cu (at. %)) under compressive loading is conducted in the present subsection. The calculated result is compared with the experimental result of Urushiyama, Lewinnek, Qiu, and Tani [9].

The material constants used in the analysis are shown in Table 2. The elastic constants and the temperatures for the phase transformation in Table 2 are from the literature [9], while the other material constants have been determined so as to fit the constitutive equation proposed in the section II with the experimental results [9]. The temperature in the analysis is  $22^\circ\text{C}$  which is lower than the temperature for finishing martensite transformation ( $M_f$ ).

Fig. 5 shows the dimensions ( $L = 50.0\text{mm}$ ,  $D = 5.0\text{mm}$ ) and the boundary conditions of the SMA column for the buckling analysis. The numbers of elements and nodes are 1000 and 1717, respectively. The SMA column model with the initial imperfections of 0.028mm is employed for the finite element analysis. The calculated and experimental load-displacement curves are shown in Fig. 7. Although the calculated result has all corresponded well with the experimental result, there is a large difference for the maximum buckling load (calculation = 14000N, experiment = 20000N). The difference is due to the fact that the buckling phenomenon is very sensitive to initial imperfection and the material constants.

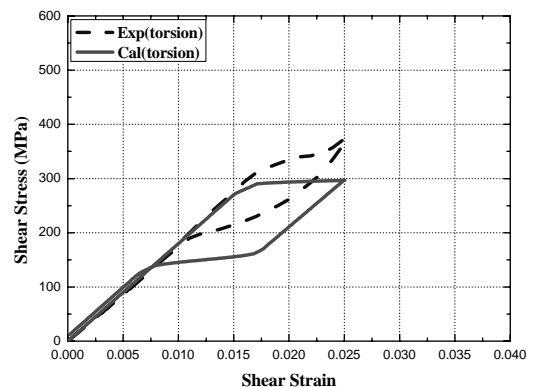


Fig. 4 Shear stress-shear strain curves of SMA microtube under pure torsion

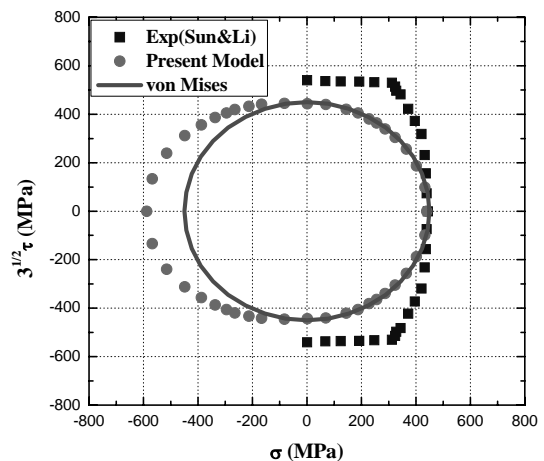


Fig. 5 Stress locus at the start of martensite transformation

Table 2 Material constants of the SMA column  
 (40.8Ni-49.3Ti-9.9Cu (at. %)) (\*: Reference [9])

|                             |                       |         |
|-----------------------------|-----------------------|---------|
| Moduli                      | $E_a$ (MPa)           | 20000 * |
|                             | $E_m$ (MPa)           | 40200 * |
|                             | $C_{M_s}$ (MPa / °C)  | 8.0     |
|                             | $C_{M_f}$ (MPa / °C)  | 8.0     |
|                             | $C_{A_s}$ (MPa / °C)  | 6.9     |
|                             | $C_{A_f}$ (MPa / °C)  | 6.9     |
|                             | $\nu$                 | 0.3     |
|                             | $\beta$               | 0.15    |
| Transformation Temperatures | $M_f$ (°C)            | 30.0 *  |
|                             | $M_s$ (°C)            | 44.6 *  |
|                             | $A_s$ (°C)            | 51.9 *  |
|                             | $A_f$ (°C)            | 64.9 *  |
| Critical stresses           | $\sigma_s^{cr}$ (MPa) | 0.0     |
|                             | $\sigma_f^{cr}$ (MPa) | 200.0   |
| Maximum residual strains    | $\epsilon_L$          | 0.04    |
|                             | $\gamma_L$            | 0.04    |

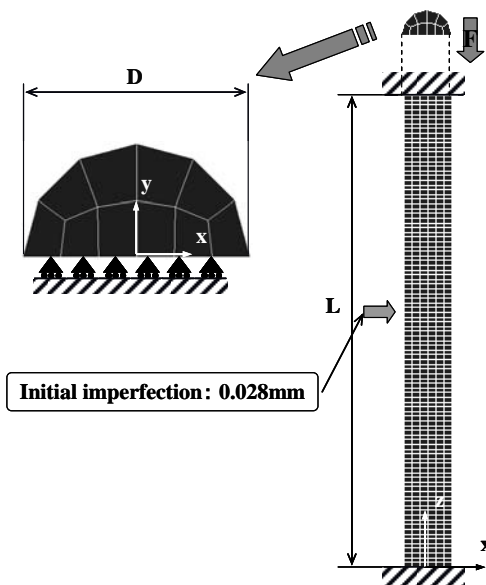


Fig. 6 Finite element model and boundary condition for the SMA column

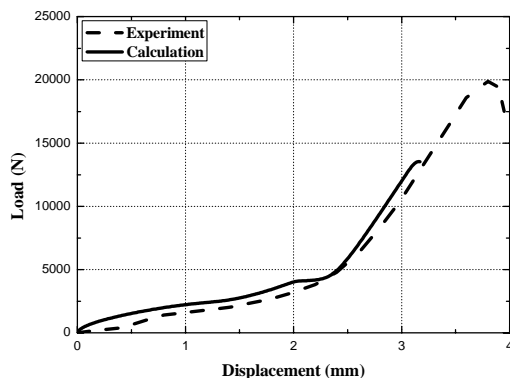


Fig. 7 Load-displacement curves of the SMA column under compressive loading

C. Superelastic behavior of the SMA stent

Stent is the technical word indicating self-expanding micro-structures, which are currently investigated for the treatment of hollow-organ or duct-system occlusions [10]. In the present subsection, the superelastic large deformation analysis of the SMA stent (Ni-Ti-10.0Cu (at. %)) being used for the medical engineering field is conducted. The calculated results are compared with the analytical results by the computational model of Auricchio and Taylor [10] which is employed in the commercial code ANSYS.

The material constants used in the analysis are shown in Table 3. The elastic constant of the austenite phase, the material parameter  $\beta$ , and the temperatures for the phase transformation in Table 3 are from the literature [10], while the other material constants have been determined so as to fit the constitutive equation proposed in the section II with the experimental stress-strain curve [10].

A stent with a diamond pattern is given in Fig. 8 with dimensions ( $L_1 = 0.35\text{mm}$ ,  $L_2 = 1.8\text{mm}$ ,  $L_3 = 0.28\text{mm}$ ,  $L_4 = 0.51\text{mm}$ ,  $\theta = 40.0^\circ$ ,  $R_{int} = 2.00\text{mm}$ ,  $R_{ext} = 2.25\text{mm}$ ). Fig. 9 shows the boundary conditions of the SMA stent for the superelastic analysis. Due to the symmetry conditions, only one quarter of a diamond pattern need to be modeled. As output parameters, the axial load F and the displacement of node V are employed either in the axial direction or in the inward radial direction. The numbers of elements and nodes are 128 and 291, respectively. A loading-unloading history with a peak load of 50N is considered. Fig. 10 and 11 show the axial load-axial displacement curves and the axial load-radial displacement curves, respectively. Although the calculated results have all corresponded well with the analytical results by Auricchio and Taylor [10], there is a slight difference at the later stage of loading and the initial stage of unloading.

Table 3 Material constants of the SMA stent  
 (Ni-Ti-10.0Cu (at. %)) (\*: Reference [10])

|                             |                       |                |
|-----------------------------|-----------------------|----------------|
| Moduli                      | $E_a$ (MPa)           | 60000 *        |
|                             | $E_m$ (MPa)           | 20000          |
|                             | $C_{M_s}$ (MPa / °C)  | 8.0            |
|                             | $C_{M_f}$ (MPa / °C)  | 8.0            |
|                             | $C_{A_s}$ (MPa / °C)  | 13.0           |
|                             | $C_{A_f}$ (MPa / °C)  | 13.0           |
|                             | $\nu$                 | 0.3            |
|                             | $\beta$               | 0.15 *         |
| Transformation Temperatures | $M_f$ (°C)            | $T_0 - 30.0$ * |
|                             | $M_s$ (°C)            | $T_0 - 44.6$ * |
|                             | $A_s$ (°C)            | $T_0 - 51.9$ * |
|                             | $A_f$ (°C)            | $T_0 - 64.9$ * |
| Critical stresses           | $\sigma_s^{cr}$ (MPa) | 100.0          |
|                             | $\sigma_f^{cr}$ (MPa) | 220.0          |
| Maximum residual strains    | $\epsilon_L$          | 0.067          |
|                             | $\gamma_L$            | 0.067          |

This difference is due to the fact that it is supposed that Young's modulus of the austenite phase and martensite phase are equal in the modeling of Auricchio and Taylor [10] ( $E_a = E_m$ ), while both moduli are assumed to be independent in the present formulation ( $E_a \neq E_m$ ).

### V. CONCLUSION

The method of finite element analysis for the multiaxial behavior of SMA elements previously formulated by the authors [7] is extended to the geometrically nonlinear analysis in the present study. The present formulation has been applied to the superelastic behavior analyses for the SMA microtube, the SMA column, and the SMA stent. The calculated results have been compared with the experimental results. The present method is valid in practice as a computational procedure for the superelastic behavior of a SMA device.

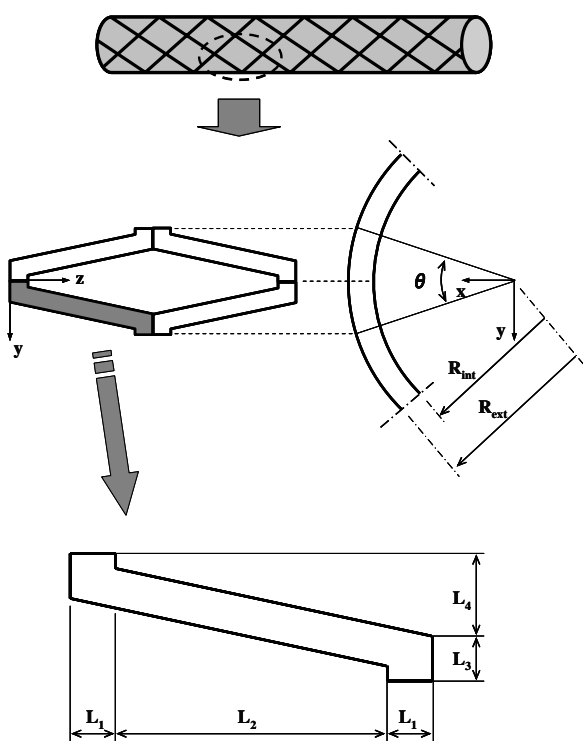


Fig. 8 Dimensions for the SMA stent

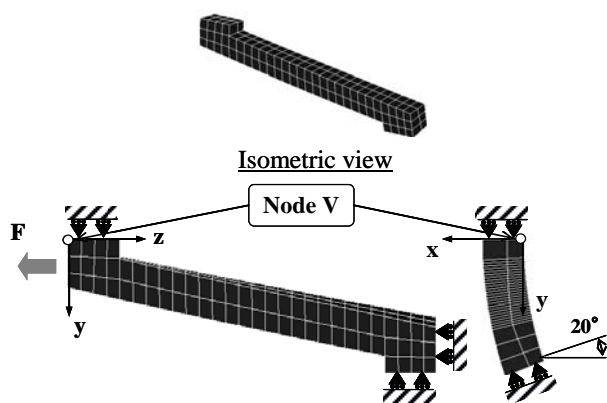


Fig. 9 Finite element model and boundary condition for the SMA stent

### REFERENCES

- [1] F. Auricchio, "A Robust Integration-Algorithm for a Finite-Strain Shape-Memory-Alloy Superelastic Model" *International Journal of Plasticity*, vol. 17, pp. 971-990, 2001.
- [2] T. J. Lim and D. L. McDowell, "Cyclic Thermomechanical Behavior of a Polycrystalline Pseudoelastic Shape Memory Alloy" *Journal of the Mechanics and Physics of Solids*, vol. 50, pp. 651-676, 2002.
- [3] W. Dettmer and S. Reese, "On the Theoretical and Numerical Modelling of Armstrong-Frederick Kinematic Hardening in the Finite Strain Regime" *Computer Methods in Applied Mechanics and Engineering*, vol. 193, pp. 87-116, 2004.
- [4] F. Auricchio and L. Petrini, "A Three-Dimensional Model Describing Stress-Temperature Induced Solid Phase Transformations: Solution Algorithm and Boundary Value Problems" *International Journal for Numerical Methods in Engineering*, vol. 61, pp. 807-836, 2004.
- [5] H. Pan, P. Thamburaja, and F. S. Chau, "Multi-Axial Behavior of Shape-Memory Alloy Undergoing Martensitic Reorientation and Detwinning" *International Journal of Plasticity*, vol. 23, pp. 711-732, 2007.
- [6] S. Reese and D. Christ, "Finite Deformation Pseudo-Elasticity of Shape Memory Alloys - Constitutive Modelling and Finite Element Implementation" *International Journal of Plasticity*, vol. 24, pp. 455-482, 2008.
- [7] Y. Toi and D. Choi, "Computational Modeling of Superelastic Behaviors of Shape Memory Alloy Devices under Combined Stresses" *Journal of Computational Science and Technology*, vol. 2, no. 4, pp. 535-546, 2008.
- [8] Q. P. Sun and Z. Q. Li, "Phase Transformation in Superelastic NiTi Polycrystalline Micro-Tubes under Tension and Torsion-from Localization to Homogeneous Deformation" *International Journal of Solids and Structures*, vol. 39, pp. 3797-3809, 2002.
- [9] Y. Urushiyama, D. Lewinnek, J. Qiu, and J. Tani, "Buckling of Shape Memory Alloy Columns (1st report, Buckling of Curved Column and Twinning Deformation Effect)" *Transactions of the Japan Society for Mechanical Engineers (A)*, vol. 67, no. 659, pp. 1132-1139, 2001.
- [10] F. Auricchio and R. L. Taylor, "Shape-Memory Alloys: Modelling and Numerical Simulations of the Finite-Strain Superelastic Behavior" *Computer Methods in Applied Mechanics and Engineering*, vol. 143, pp. 175-194, 1997.

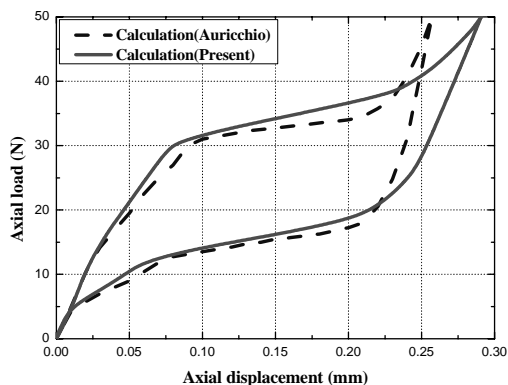


Fig. 10 Axial load-axial displacement curves

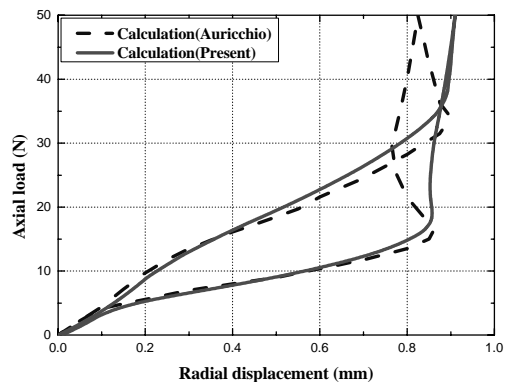


Fig. 11 Axial load-radial displacement curves